p97/VCP Promotes the Recycling of Endocytic Cargo

Mona Kawan[a], Maria Körner[a], Andreas Schlosser[b] and Alexander Buchberger[a,*]
[a]Chair of Biochemistry I, University of Würzburg, Biocenter, Am Hubland, 97074 Würzburg, Germany;
[b]Rudolf Virchow Center for Integrative and Translational Bioimaging, University of Würzburg, Josef-Schneider-Straße 2, 97080 Würzburg, Germany

ABSTRACT **The endocytic pathway is of central importance for eukaryotic cells, as it enables uptake of extracellular materials, membrane protein quality control and recycling, as well as modulation of receptor signaling. While the ATPase p97 (VCP, Cdc48) has been found to be involved in the fusion of early endosomes and endolysosomal degradation, its role in endocytic trafficking is still incompletely characterized. Here, we identify myoferlin (MYOF), a ferlin family member with functions in membrane trafficking and repair, as a hitherto unknown p97 interactor. The interaction of MYOF with p97 depends on the cofactor PLAA previously linked to endosomal sorting. Besides PLAA, shared interactors of p97 and MYOF comprise several proteins involved in endosomal recycling pathways, including Rab11, Rab14, and the transferrin receptor CD71. Accordingly, a fraction of p97 and PLAA localizes to MYOF-, Rab11-, and Rab14-positive endosomal compartments. Pharmacological inhibition of p97 delays transferrin recycling, indicating that p97 promotes not only the lysosomal degradation, but also the recycling of endocytic cargo.**

SIGNIFICANCE STATEMENT

- The ATPase p97/VCP has been linked to endosomal trafficking in the past, but the full range of its involvement in endosomal processes is still unknown.
- The authors used crosslinking-assisted mass spectrometry to identify MYOF as novel p97 binding partner.
- Using immunofluorescence microscopy, they found that a subpopulation of p97 and MYOF localizes to recycling endosomes and that chemical inhibition of p97 delays the recycling of transferrin to the plasma membrane.
- These findings suggest that p97 possesses functions beyond the endolysosomal degradation of endocytic cargo and implicate p97 in MYOF-dependent membrane trafficking and repair pathways.

Monitoring Editor
Michael Rape
University of California, Berkeley

Received: Jun 20, 2023
Revised: Sep 11, 2023
Accepted: Sep 20, 2023

This article was published online ahead of print in MBoC in Press (http://www.molbiolcell.org/cgi/doi/10.1091/mbc.E23-06-0237) on September 27, 2023.

Conflict of interest: The authors declare no competing interests.

Author contributions: M.Ka. and A.B. conceived the project and wrote the manuscript; M.Ka. and M.Kö. performed experiments; M.Ka., M.Kö., A.S. and A.B. analyzed the data.

Additional information: Correspondence and requests for materials should be addressed to A.B.

*Address correspondence to: Alexander Buchberger (alexander.buchberger@uni-wuerzburg.de).

Abbreviations used: AAA, ATPases associated with diverse cellular activities; DSP, dithiobis[succinimidyl propionate]; FDR, false discovery rate; RT, room temperature; TBST, Tris-based saline with Tween.

INTRODUCTION

The maintenance of proteome homeostasis (proteostasis) is crucial for cellular and organismal health. Therefore, organisms from all domains of life rely on extensive protein quality control networks consisting of a large arsenal of molecular chaperones and proteolytic systems (Buchberger *et al.*, 2010; Labbadia and Morimoto, 2015; Balchin *et al.*, 2016). In eukaryotic cells, major systems for regulated intracellular proteolysis include the ubiquitin proteasome system, the endolysosomal degradation pathway, and selective autophagy (Hershko and Ciechanover, 1992; Clague and Urbe, 2010; Dikic, 2017; Lamark and Johansen, 2021).

The abundant and highly conserved AAA+-type ATPase p97 (also known as VCP and Cdc48) plays a key role in eukaryotic proteostasis. p97 is involved in various proteasomal degradation pathways including ER-, chromatin-, outer mitochondrial membrane-, and ribosome-associated degradation (Ye *et al.*, 2001; Tanaka *et al.*, 2010; Brandman *et al.*, 2012; Dantuma and Hoppe, 2012); in the selective autophagy of aggregates, stress granules, and damaged organelles (Ju *et al.*, 2008; Tanaka *et al.*, 2010; Buchan *et al.*, 2013; Kim *et al.*, 2013; Papadopoulos *et al.*, 2017); and in the lysosomal degradation of endocytic cargo (Ritz *et al.*, 2011). These diverse cellular functions are mediated by more than 30 regulatory cofactors that control substrate binding, subcellular localization, and oligomeric state of p97 (Buchberger *et al.*, 2015). Mechanistically, p97 uses the energy from ATP hydrolysis to processively unfold substrate proteins, thereby segregating them from protein complexes, membranes, or chromatin to release them for their respective downstream fates (Bodnar and Rapoport, 2017; van den Boom and Meyer, 2018; Buchberger, 2022).

The central importance of p97 for the maintenance of protein and organelle homeostasis is underscored by the fact that missense mutations in the *VCP* gene encoding human p97 cause the complex, neuromuscular degenerative disease multisystem proteinopathy 1 (MSP1; formerly known as inclusion body myopathy with Paget disease of the bone and frontotemporal dementia and familial amyotrophic lateral sclerosis, or IBMPFD/fALS; Watts *et al.*, 2004; Johnson *et al.*, 2010; Pfeffer *et al.*, 2022). While p97-dependent processes and target proteins critical for the pathogenesis of MSP1 are still incompletely understood, accumulating evidence suggests that impaired lysosomal degradation of autophagic and endocytic cargo plays an important role. Thus, p97 is required for the efficient clearance of stress granules, and cells expressing disease-causing mutant p97 exhibit clearance defects that have been implicated in the pathological formation of insoluble protein aggregates (Buchan *et al.*, 2013; Rodriguez-Ortiz *et al.*, 2016; Turakhiya *et al.*, 2018; Wang *et al.*, 2019). Similarly, the failure of disease-causing mutant p97 to efficiently mediate the removal of damaged lysosomes and mitochondria via selective autophagy has been found to correspond to the accumulation of such damaged organelles in cellular and animal models of MSP1 and, in the case of lysosomes, in patient muscle tissue (Kim *et al.*, 2013; Papadopoulos and Meyer, 2017; Zhang *et al.*, 2017). Finally, disease-causing mutant p97 has been shown to interfere with normal endolysosomal trafficking, resulting in the accumulation of caveolins 1 and 3 in MSP1 cellular models, patient fibroblasts, and muscle tissue (Ritz *et al.*, 2011).

The endolysosomal degradation pathway (reviewed in Huotari and Helenius, 2011; Cullen and Steinberg, 2018) starts with the internalization of extracellular material and plasma membrane (PM) proteins through clathrin-dependent and -independent mechanisms. The endocytic vesicles subsequently undergo homotypic fusion in the peripheral cytoplasm to form early endosomes (EEs), which consist of distinct tubular and vacuolar domains and act as major sorting hubs for endocytic cargo. Ubiquitylated membrane proteins destined for lysosomal degradation, such as activated growth factor receptors, are sorted into intraluminal vesicles (ILVs) inside the vacuolar domain of EEs by the ordered action of four different ESCRT complexes and the ATPase VPS4 (Raiborg and Stenmark, 2009), a process that continues during the maturation of EEs into late endosomes (LEs; also known as multivesicular bodies). LEs are transported along microtubules to the perinuclear area of the cell, where they fuse with each other and with lysosomes to form endolysosomes. The ILVs carrying endocytosed cargo are degraded inside the endolysosomes by lysosome-derived hydrolases. Of note, only a relatively small fraction of endocytosed proteins is actively sorted into ILVs for endolysosomal degradation (Huotari and Helenius, 2011), whereas the majority of internalized cargo is recycled from tubular domains of EEs back to the PM, either directly or via recycling endosomes (REs; Grant and Donaldson, 2009; Huotari and Helenius, 2011). Importantly, the identity of the different endosomal compartments is largely determined by distinct Rab GTPases and their effector proteins (Wandinger-Ness and Zerial, 2014; Langemeyer *et al.*, 2018; Lamber *et al.*, 2019). While EEs are defined by the presence of Rab5, a "Rab switch" from Rab5 to Rab7 during EE maturation reprograms the association of effector proteins and, hence, the properties of LEs. The different endocytic recycling routes are governed by distinct Rab proteins. Rab4 is required for fast recycling from EEs to the PM (van der Sluijs *et al.*, 1992), whereas recycling via REs or (in some cell types) a perinuclear endosomal recycling compartment (ERC) is controlled by Rab11 and Rab14, with Rab14 defining an intermediate step between EEs and Rab11-positive REs (Ullrich *et al.*, 1996; Linford *et al.*, 2012).

While p97 has been implicated in different steps of the endolysosomal pathway, including the fusion of EEs (Ramanathan and Ye, 2012) and the endolysosomal sorting and degradation of endocytic cargo (Ritz *et al.*, 2011), our understanding of the role(s) of p97 in endocytic trafficking is still far from complete. Here, we report the identification of the ferlin family member myoferlin (MYOF) as a novel p97 interactor. We show that the interaction between MYOF and p97 depends on the p97 cofactor PLAA and that p97, PLAA, and MYOF partially colocalize at Rab14- and Rab11-positive endosomal structures. Finally, we demonstrate that pharmacological inhibition of p97 leads to its partial localization to REs and delay the recycling of endocytosed cargo, indicating that p97 plays roles in the endocytic pathway beyond lysosomal degradation by promoting endocytic recycling.

RESULTS

Proteomic analysis of the dynamic p97 interactome

In an effort to identify unknown p97-binding partners, we sought to determine the interactome of endogenous, untagged p97 in HeLa cells using affinity purification followed by mass spectrometry. However, the interactions of p97 with regulatory cofactors and presumably also other proteins are highly dynamic and thus difficult to catch by conventional proteomics approaches (Xue *et al.*, 2016). Therefore, we stabilized the p97 interactome *in cellulo* using the homobifunctional, reducible crosslinker dithiobis[succinimidyl propionate] (DSP; Xue *et al.*, 2016). At a final concentration of 0.8 mM, DSP converted most, but not all cellular p97 into sodium dodecyl sulfate (SDS)-resistant, high molecular-weight complexes that readily disappeared upon addition of dithiothreitol (DTT; Supplemental Figure S1A), suggesting that p97 was efficiently crosslinked, but not over-crosslinked. After crosslinking and cell lysis, we immunoprecipitated endogenous p97 complexes and performed label-free

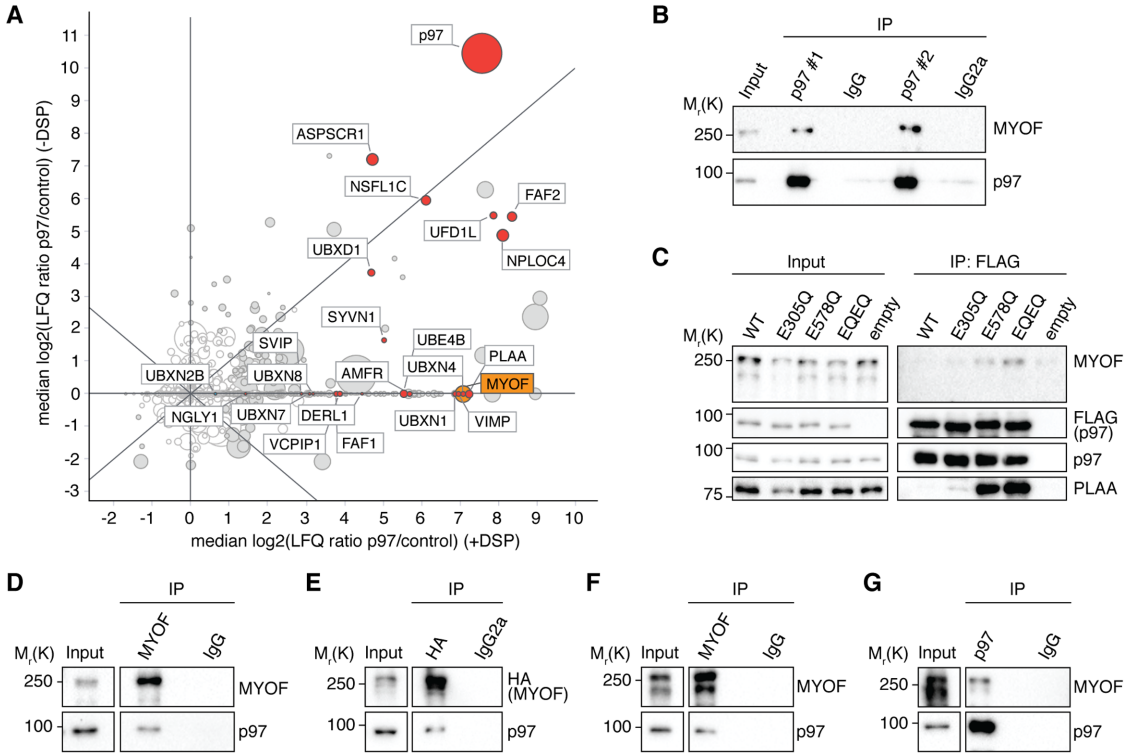

FIGURE 1: MYOF is a novel p97 interactor. (A) p97 interactome analysis. HeLa cells were treated with the crosslinker dithiobis[succinimidyl propionate] (+DSP) or left untreated (–DSP). Endogenous p97 was immunoprecipitated and analyzed for coprecipitated proteins by label-free quantitative mass spectrometry. The plot shows the medians of the enrichment ratios for p97 versus IgG control IPs in the presence (x-axis) and absence (y-axis) of DSP, respectively; $n = 3$. Circle diameters correlate with the sum of identified razor and unique peptides. p97 cofactors and MYOF are marked in red and orange, respectively. (B) Validation of the MYOF interaction. Lysates of DSP-treated HeLa cells were subjected to IP with two different p97 antibodies or with matched unspecific IgGs as indicated, followed by immunoblotting against MYOF and p97. (C) MYOF interacts with p97 in the absence of crosslinker. Lysates of HeLa cell pools ectopically expressing the indicated FLAG epitope-tagged wild-type or mutant p97 variants or carrying empty vector control were subjected to anti-FLAG IP, followed by immunoblotting against MYOF, FLAG, p97, and PLAA. (D) p97 coprecipitates with MYOF. Lysates of DSP-treated HeLa cells were subjected to IP with a MYOF antibody or unspecific IgGs, followed by immunoblotting against MYOF and p97. (E–G) p97 and MYOF interact in HEK293T cells. HEK293T cells ectopically expressing MYOF–HA were treated with DSP. The cell lysate was split and subjected to IPs with antibodies directed against the HA epitope tag (E), MYOF (F), and p97 (G), respectively, followed by immunoblotting against HA, MYOF, and p97 as indicated.

quantitative mass spectrometry (Supplemental Tables S2 and S3). To assess the effect of crosslinking, we compared the p97 interactomes obtained in the absence and presence of DSP and initially focused on p97 cofactors, which have been previously reported to cover a range of binding kinetics (Xue *et al.*, 2016). The binding of six cofactors (ASPSCR1, NSFL1C/p47, UBXD1, UFD1L, NPLOC4, and FAF2) was not or only moderately stabilized by DSP, as indicated by their positions close to the diagonal of the plot (Figure 1A). By contrast, a larger number of cofactors were exclusively detected in the presence of DSP, in agreement with a recent analysis of the p97 interactome in HEK293 cells and BJ fibroblasts (Xue *et al.*, 2016). Thus, our results confirm that in-cell crosslinking with DSP is able to preserve unstable, bona fide physiologic protein–protein interactions of p97 during cell lysis and immunoprecipitation (IP).

MYOF is a novel p97 interactor

We next turned our attention to candidates exclusively detected after in-cell crosslinking with DSP, as these are unlikely to represent postlysis or unspecific interactors, and identified MYOF as one of the most strongly enriched proteins (Figure 1A, orange circle). To validate this finding, we immunoprecipitated endogenous p97 from a DSP-crosslinked HeLa cell lysate using two different p97 antibodies and found that MYOF was specifically coprecipitated (Figure 1B), confirming the mass spectrometry data. Because the p97–MYOF complex could not be immunoprecipitated in the absence of DSP (Figure 1A), we sought to further validate the interaction by using ATPase-deficient p97 variants known to trap p97 complexes (Ye *et al.*, 2003). To that end, we generated stable HeLa cell pools inducibly expressing FLAG epitope-tagged wild-type p97 or p97 variants mutated in the Walker B motif of the D1 domain (E305Q), the D2 domain (E578Q), or both domains (EQEQ; Supplemental Figure S1B). In FLAG immunoprecipitates from noncrosslinked lysates of these cell pools, MYOF coprecipitated with p97 complexes containing the E578Q or EQEQ traps, but hardly above background with p97 complexes containing E305Q (Figure 1C, Supplemental Figure S1C). Similar to MYOF, the p97 cofactor PLAA, which was detected in the p97 interactome exclusively upon DSP crosslinking (Figure 1A), efficiently coprecipitated with the p97 E578Q and EQEQ traps, consistent with previous reports (Ritz *et al.*, 2011; Papadopoulos *et al.*, 2017). To further validate MYOF as a novel p97-binding protein, we performed reciprocal IPs of endogenous MYOF from DSP-crosslinked HeLa and A549 cells and detected a specific coprecipitation of p97 (Figure 1D, Supplemental

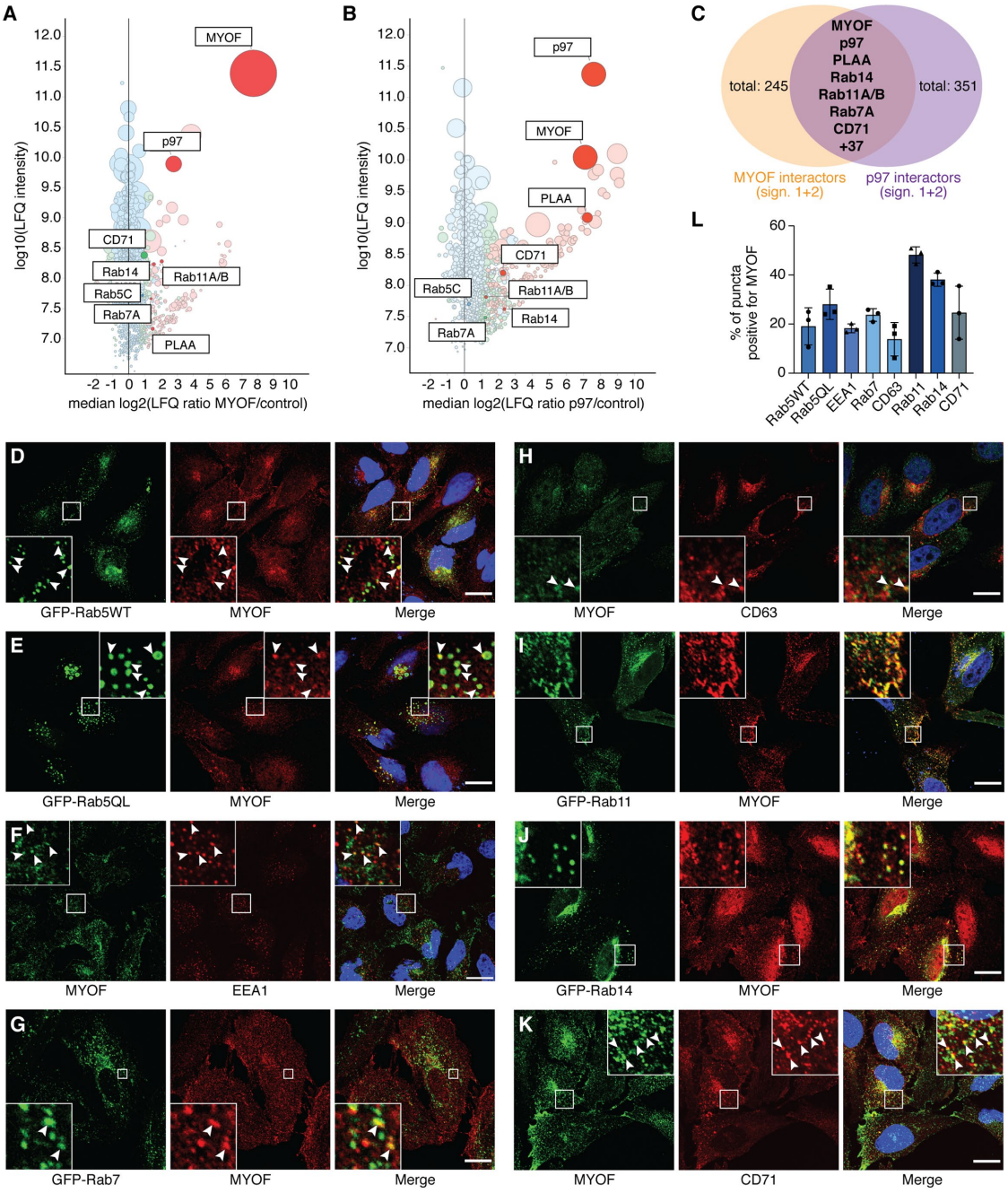

FIGURE 2: MYOF localizes to early, late, and recycling endocytic compartments. (A and B) Comparative analysis of MYOF and p97 interactomes. HeLa cells were subjected to cross-linking with DSP and IP of endogenous MYOF (A) and p97 (B), respectively, followed by label-free quantitative mass spectrometry. Circle diameters correlate with the number of identified razor and unique peptides; $n = 3$. Interactors are color coded according to significance levels 0 (blue), one (green) and two (red). Selected shared interactors of MYOF and p97 are labeled. (C) Venn diagram showing shared MYOF and p97 interactors (significance levels one and two) linked to the endosomal system. (D–K) Localization of MYOF to endocytic compartments. Confocal immunofluorescence microscopy of HeLa cells costained for endogenous MYOF and ectopically expressed GFP-Rab5WT (D), GFP-Rab5QL (E), endogenous EEA1 (F), ectopically expressed GFP-Rab7 (G), endogenous CD63 (H), ectopically expressed GFP-Rab11 (I), GFP-Rab14 (J), and endogenous CD71 (K), respectively. In the blowups of (D), (E), (F), (G), (H), and (K), representative examples for the colocalization of MYOF with the respective marker proteins are highlighted by arrowheads. Scale bars, 20 µm. (L) Quantification of colocalization between MYOF and the endosomal markers shown in panels D–K. $n = 3$ biological replicates with 15–45 cells quantified per condition and replicate. Shown is mean ± SD.

Figure S1D). Finally, we ectopically expressed HA epitope-tagged MYOF in HEK293T cells (which express very low levels of endogenous MYOF), performed in-cell crosslinking and subjected the lysate to parallel IPs using antibodies against the HA tag, MYOF, and p97, respectively (Figure 1, E–G). In all three immunoprecipitates, the co-precipitation of p97 and MYOF was observed. Taken together, our

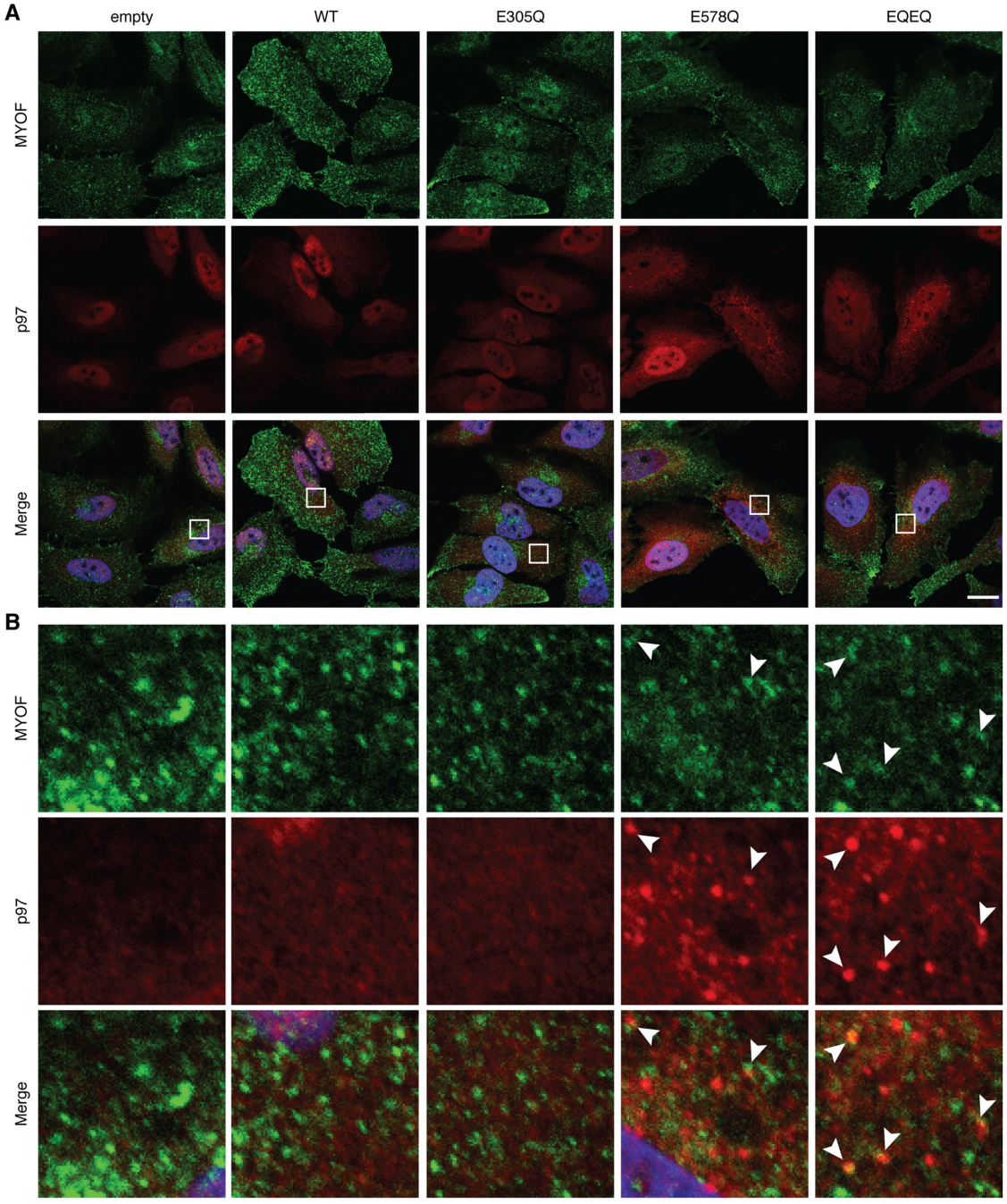

FIGURE 3: p97 partially colocalizes with MYOF. (A) Stable HeLa cell pools ectopically expressing the indicated wild-type or mutant, FLAG epitope-tagged p97 variants were stained for p97 and endogenous MYOF and subjected to confocal immunofluorescence microscopy. Scale bar, 20 μm. (B) Blowups of the areas marked in A. Colocalization of p97 and MYOF in cells expressing the p97 E578Q and EQEQ trapping mutants is highlighted by arrowheads.

data demonstrate an interaction between MYOF and endogenous p97 in three different cell lines after in-cell crosslinking, as well as upon expression of p97 trapping mutants in the absence of crosslinker, thus establishing MYOF as a novel p97 interactor.

MYOF localizes to early, late, and recycling endosomal compartments

The ferlin family member MYOF is a 230 kDa, tail-anchored membrane protein comprising ferlin homology and multiple C2 domains involved in membrane tethering (Bulankina and Thoms, 2020). MYOF was initially found to be involved in myoblast fusion during embryonic development, skeletal muscle regeneration, and repair (Doherty *et al.*, 2005; Demonbreun *et al.*, 2010a, 2010b), but has since been implicated in multiple trafficking events along the secretory and endocytic pathways (Doherty *et al.*, 2008; Bernatchez *et al.*, 2009; Demonbreun *et al.*, 2010b; Turtoi *et al.*, 2013; Redpath *et al.*, 2016; Bulankina and Thoms, 2020). To get further insights into the significance of the interaction between p97 and MYOF, we determined the interactome of endogenous MYOF after in-cell crosslinking and compared it to the p97 interactome described above (Figure 2, A–C). Besides p97, a number of proteins with functions in endocytic trafficking were identified as MYOF interactors (Figure 2A;

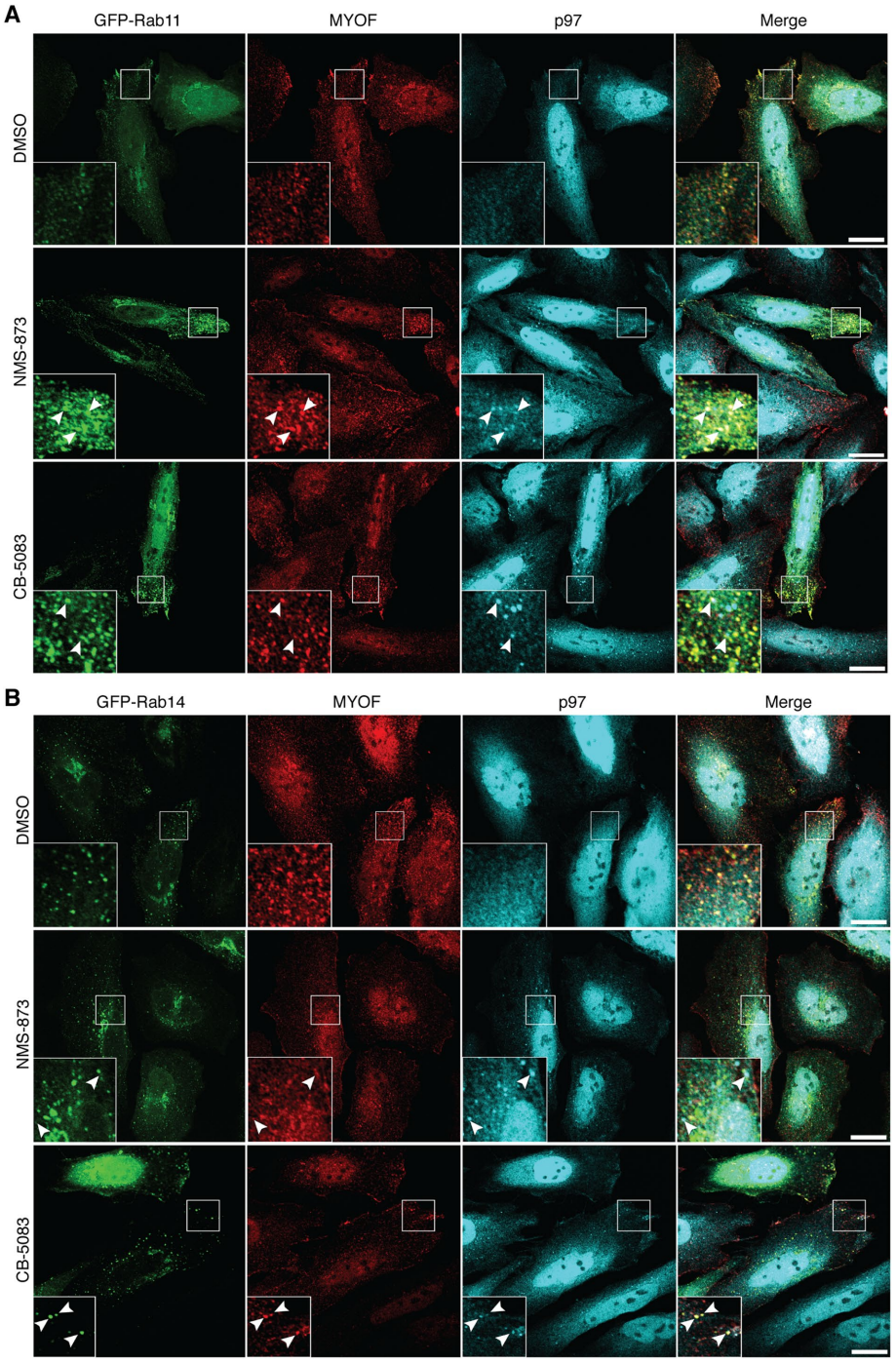

FIGURE 4: p97 and MYOF colocalize at Rab11- and Rab14-positive compartments. (A and B) HeLa cells ectopically expressing GFP-Rab11 (A) or GFP-Rab14 (B) were incubated for 3 h with vehicle (DMSO) or with the p97 inhibitors NMS-873 or CB-5083 (10 μM) and subjected to confocal immunofluorescence microscopy for the detection of endogenous p97, endogenous MYOF, and Rab11 (A) or Rab14 (B), respectively. Colocalization of p97 with MYOF and Rab11/Rab14 is highlighted by arrowheads in the blowups. Scale bars, 20 μm.

Supplemental Tables S2 and S4) and, intriguingly, several of these proteins were also present in the p97 interactome (Figure 2B). At the two highest significance levels, shared interactors included the p97 cofactor PLAA, the endosomal Rab proteins Rab14, Rab11, and Rab7, the transferrin receptor CD71 (also known as Transferrin receptor 1, TfR1), and 37 additional proteins (Figure 2C; Supplemental Table S2). The early endosomal protein Rab5 was also identified in both interactomes, albeit with lower significance. These results suggested the possibility that MYOF and p97 are both present at endosomal compartments. Because the subcellular localization of endogenous MYOF had so far not been analyzed systematically in HeLa cells, we performed confocal immunofluorescence microscopy using antibodies specifically detecting MYOF (Supplemental Figure S2, A and B) in combination with various markers of endosomal compartments. We found that endogenous MYOF was present in punctate, presumably vesicular structures that colocalized to varying extents with the early endosomal markers Rab5 (wild-type and constitutively active mutant; Figure 2, D and E) and EEA1 (Figure 2F), with the late endosomal marker Rab7 (Figure 2G) and with the lysosomal marker CD63 (Figure 2H). A strong colocalization was observed with Rab11 (Figure 2I) and Rab14 (Figure 2J), indicating that MYOF is not only present at compartments of the endolysosomal pathway, but also at REs. In support of this conclusion, MYOF also colocalized with CD71, a well-established cargo of endocytic recycling pathways (Figure 2K). Plot profiles confirmed the partial colocalization of MYOF with the endocytic markers (Supplemental Figure 3), and an object-based quantification of colocalization revealed that MYOF indeed localized to about 40% of the Rab14- and 50% of the Rab11-positive puncta, respectively (Figure 2L).

p97 colocalizes with MYOF at recycling endosomal compartments

Next, we investigated whether p97 colocalizes with MYOF. To that end, we performed confocal immunofluorescence microscopy of HeLa cell pools expressing the dominant-negative p97 trapping mutants, using an antibody that specifically detects p97 (Supplemental Figure S2, C–E). Upon ectopic expression of wild-type p97 or the D1 mutant E305Q, no costaining could be observed between the punctate pattern of MYOF-positive vesicular structures and the diffuse and granular p97 signal (Figure 3). By contrast, and consistent with their stabilizing effect in the IP experiments described above, expression of the trapping mutants E578Q and EQEQ resulted in the formation of punctate, p97-positive structures that partially colocalized with MYOF (Figure 3, A and B; Supplemental Figure S4). These punctate structures could be costained by FLAG and p97 antibodies, confirming that they contain trapped p97 complexes (Supplemental Figure S2E). Similar results were obtained for endogenous p97 in parental HeLa cells treated with the pharmacological p97 inhibitors NMS-873 and CB-5083 (Magnaghi *et al.*, 2013;

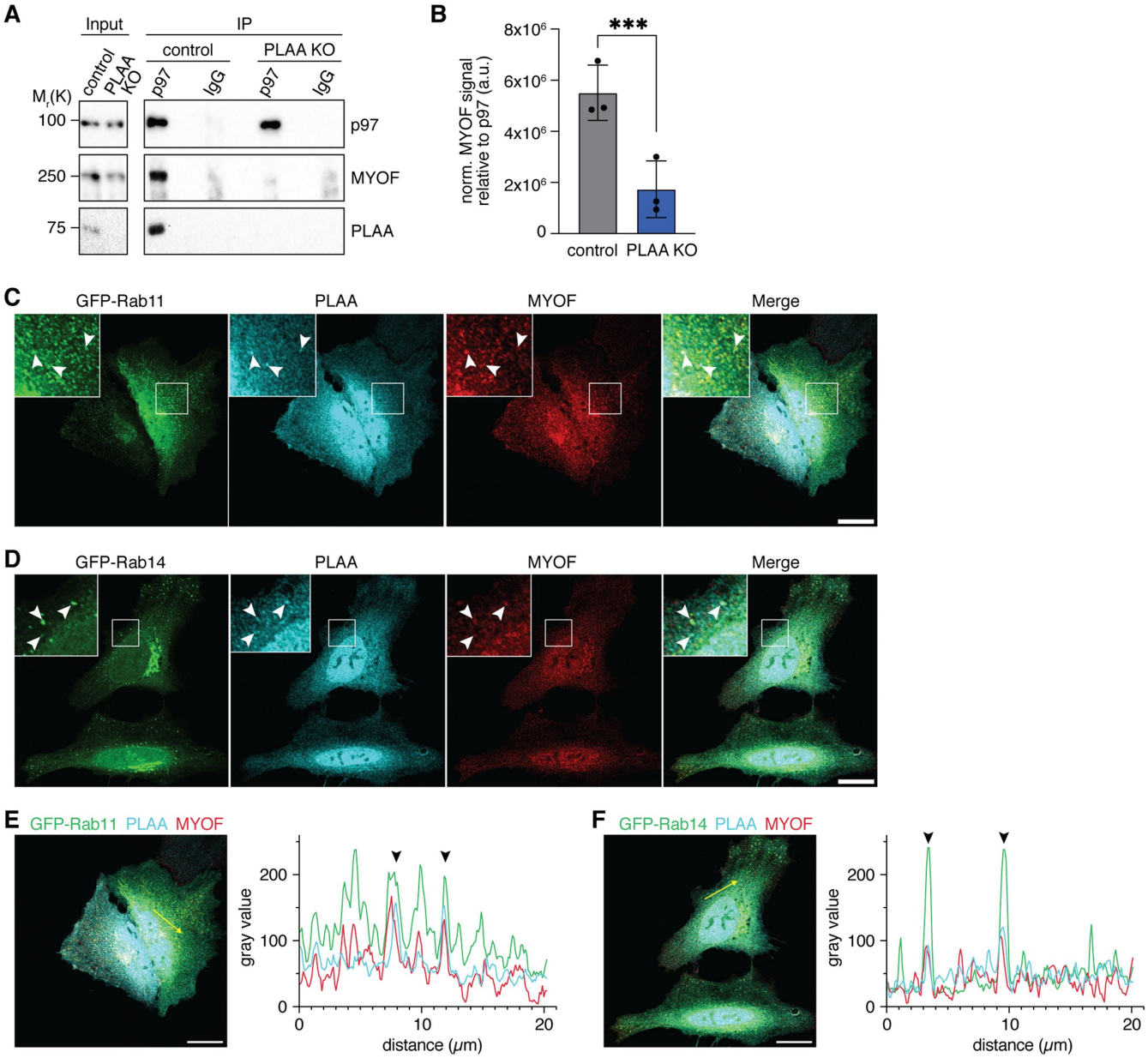

FIGURE 5: The p97 cofactor PLAA and MYOF partially colocalize at early- and recycling-endocytic compartments. (A) The interaction of p97 and MYOF depends on PLAA. CRISPR-engineered PLAA KO and control HeLa cell pools were treated with DSP and subjected to IP with a p97 antibody or with unspecific IgGs as indicated, followed by immunoblotting against p97, MYOF, and PLAA. (B) Quantification of the results shown in A. The MYOF signals in the p97 IPs were normalized to the signal of immunoprecipitated p97 in the same lane. Shown is the mean ± SD; $n = 3$ biological replicates, *t* test (two-tailed, paired, equal variance), ***$p < 0.001$. (C, D) Confocal immunofluorescence microscopy of HeLa cells ectopically expressing GFP-Rab11 (C) or GFP-Rab14 (D), costained for endogenous PLAA and MYOF. Colocalization of PLAA and MYOF with Rab11/Rab14 is marked with arrow heads in the blowups. (E and F) Plot profiles (right panels) were generated along the yellow arrows in the merged images shown in C and D, respectively (left panels). The line colors of the plots correspond to the three channels of the immunofluorescence image. Peaks overlapping in all three channels are marked with black arrowheads. Scale bars, 20 μm.

Anderson *et al.*, 2015), which inhibit the ATPase activity of p97 by different mechanisms and thereby stabilize the association of p97 with cofactors, substrates, and subcellular structures (Her *et al.*, 2016; Xue *et al.*, 2016; Huang *et al.*, 2018). While hardly any colocalization of endogenous p97 and MYOF was detected in DMSO-treated control cells, both inhibitors induced the formation of p97-positive punctate structures that showed partial colocalization with MYOF (Supplemental Figure S5). Given the strong colocalization of MYOF with Rab11- and Rab14-positive structures (Figure 2, I and J), we next tested whether endogenous p97 and MYOF colocalize at these structures in the presence of p97 inhibitors (Figure 4). Intriguingly, several of the p97 puncta induced by the inhibitors were found to costain for both MYOF and GFP-Rab11 (Figure 4A; Supplemental Figure S6, A–C; in 10%–20% of the cells) or GFP-Rab14 (Figure 4B; Supplemental Figure S6, D and E; in up to 10% of the cells), respectively. Thus, a subpopulation of p97 localizes to vesicles that are

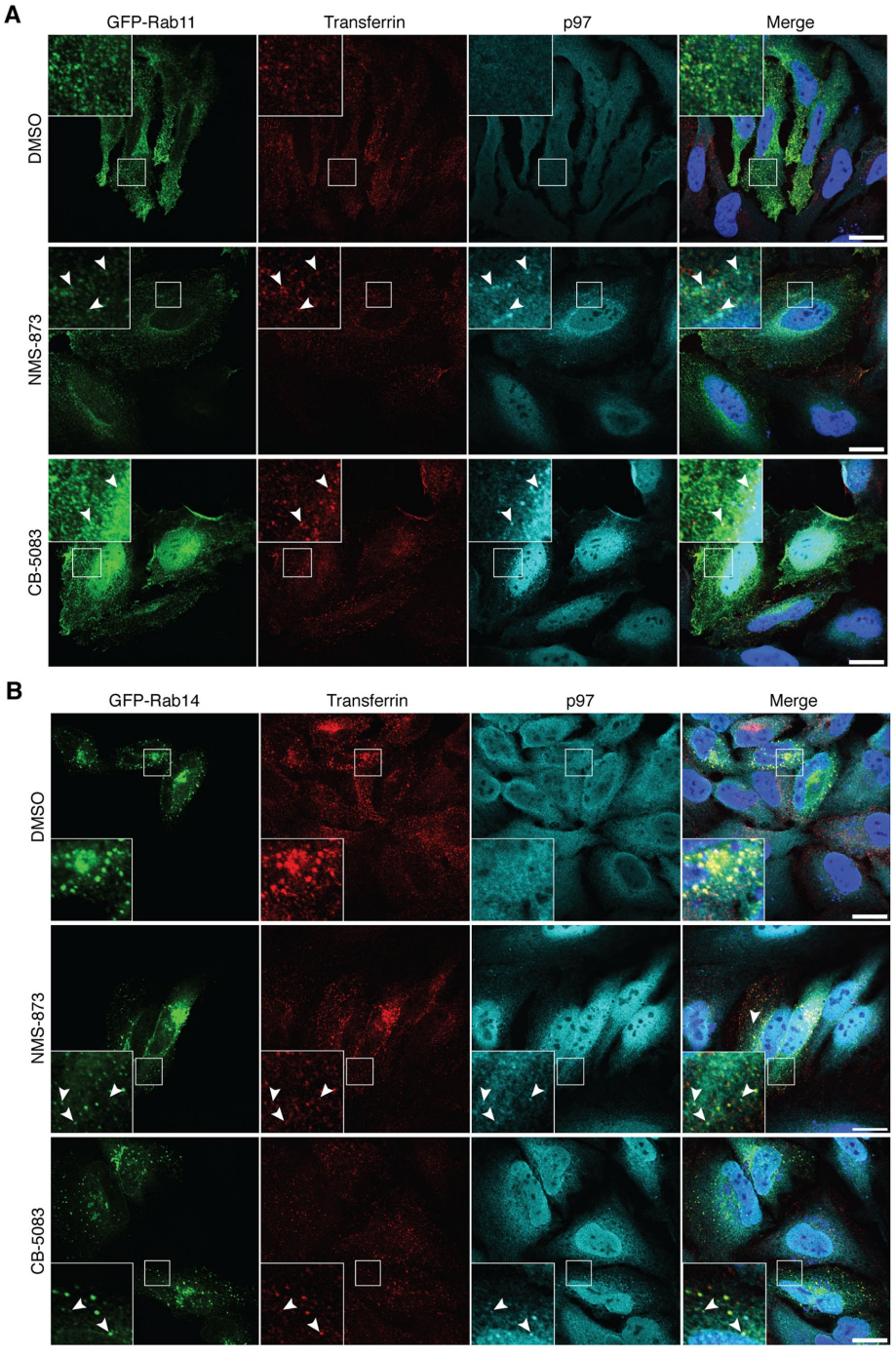

FIGURE 6: p97 localizes to REs. (A and B) HeLa cells ectopically expressing Rab11-GFP (A) or Rab14-GFP (B) were treated with vehicle (DMSO) or with the p97 inhibitors NMS-873 or CB-5083 (10 μM) for 3 h and labeled with a fluorescent Tf conjugate for 30 min. Confocal immunofluorescence microscopy detecting p97, Tf, and Rab11 (A) or Rab14 (B), respectively. Colocalization of p97 with Tf and Rab11/Rab14 is highlighted by arrowheads in the blowups. Scale bars, 20 μm.

positive for MYOF and Rab11 or Rab14, indicating that p97 and MYOF associate with REs.

PLAA mediates the interaction between p97 and MYOF

Protein–protein interactions of p97 are usually controlled by cofactors (Buchberger *et al.*, 2015). PLAA, which has recently been implicated in the endolysosomal degradation pathway (Hall *et al.*, 2017), was the only cofactor identified as shared interactor of p97 and MYOF with high significance in our proteomic analyses (Figure 2, A–C). To test for a potential involvement of PLAA in the interaction between p97 and MYOF, we performed p97 IPs using DSP-crosslinked lysates of control and PLAA knockout (KO) HeLa cell pools (Figure 5, A and B). Intriguingly, the amount of MYOF coprecipitating with p97 was reduced by more than 60% in the absence of PLAA. Together with the parallel enrichment of PLAA and MYOF observed in immunoprecipitates of p97 trapping mutants (Figure 1C), these data suggest an important role of PLAA for the binding of MYOF to p97. We therefore tested whether PLAA, like p97, colocalizes with MYOF at REs, using HeLa cells expressing GFP-Rab11 or GFP-Rab14 and an antibody specifically recognizing PLAA in immunofluorescence experiments (Supplemental Figure S2F). A small fraction of PLAA associated indeed with endosomal structures positive for Rab11 and Rab14, respectively, as well as for MYOF (Figure 5, C–F). Taken together, these data show that PLAA mediates the interaction between p97 and MYOF and partially colocalizes with MYOF at REs.

p97 localizes to REs and promotes transferrin recycling

Tf and its receptor CD71 are well-studied cargos for Rab14- and Rab11-dependent endocytic recycling. In this recycling pathway, CD71 binds extracellular iron-loaded Tf, and the complex is internalized by clathrin-mediated endocytosis. After the release of ferric iron in EEs, the Tf–CD71 complex is transported back via Rab14- and Rab11-positive vesicles to the PM, where Tf is released (Grant and Donaldson, 2009; Linford *et al.*, 2012; Mayle *et al.*, 2012; Wandinger-Ness and Zerial, 2014). Given the partial colocalization of p97 and PLAA with Rab11 and Rab14, we next tested whether p97 associates with actively REs. To that end, we labeled HeLa cells for 30 min with a fluorescent Tf conjugate and determined its colocalization with p97 and Rab11 (Figure 6A) or Rab14 (Figure 6B) in the absence and presence of p97 inhibitors. In DMSO-treated cells, Tf frequently colocalized with Rab11 and Rab14, as expected, whereas p97 signals were diffusely distributed and did not costain Tf-positive REs. By contrast, in the presence of NMS-873 or CB-5083, p97 was additionally present in punctate structures, some of which were double-positive for Tf and Rab11 or Rab14, respectively, and therefore represented bona fide REs (Figure 6, A and B, arrowheads; Supplemental Figure S7).

To test whether p97 plays a functional role in endocytic recycling, we monitored the recycling of Tf in the presence and

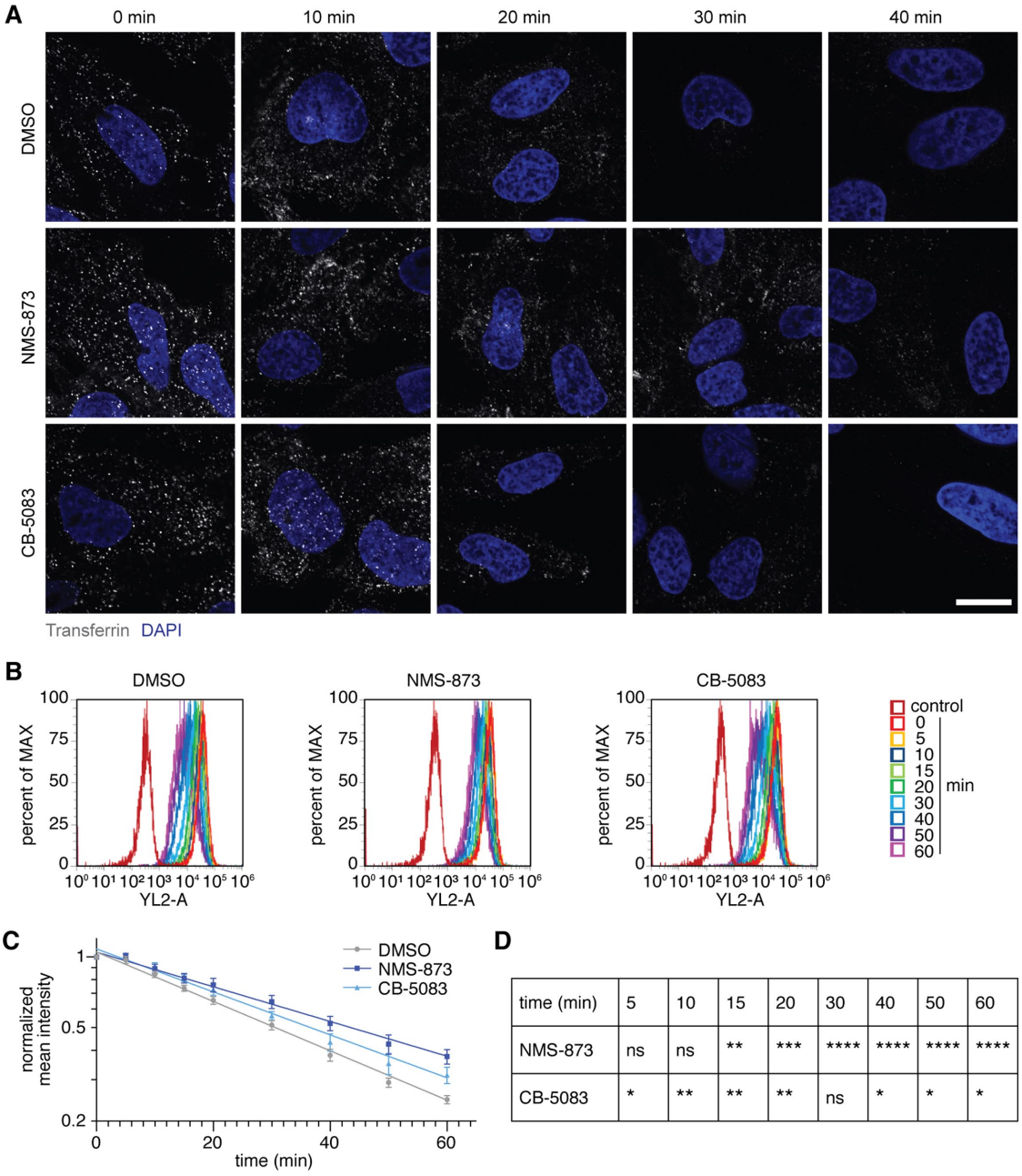

time (min)	5	10	15	20	30	40	50	60
NMS-873	ns	ns	**	***	****	****	****	****
CB-5083	*	**	**	**	ns	*	*	*

FIGURE 7: Inhibition of p97 impairs transferrin recycling. (A) HeLa cells treated with vehicle (DMSO) or with the p97 inhibitors NMS-873 or CB-5083 (10 μM) for 4 h were incubated with fluorescently labeled Tf for 5 min, washed, and chased with prewarmed growth medium for the indicated times, followed by confocal microscopy detecting Tf and DAPI. Scale bar, 10 μm. (B) HeLa cells treated with vehicle (DMSO) or with the p97 inhibitors NMS-873 or CB-5083 (10 μM) for 3.5 h were harvested, incubated with fluorescently labeled Tf, washed, chased in prewarmed growth medium containing DSMO, NMS-873 or CB-5083, respectively, and subjected to FACS analysis. The plots show overlays of the Tf signals detected in the YL2-A channel at the indicated, rainbow color-coded timepoints. (C) Quantification of the peak intensities from B. $n = 3$ biological replicates. For each timepoint, the mean ± SD of the peak intensity normalized to the zero timepoint at the respective condition is shown. The data points were plotted semilogarithmically and fitted to single exponential decay functions. (D) Two-way ANOVA of the data shown in C); Bonferroni's test was applied to correct for multiple comparisons; *$p < 0.05$, **$p < 0.01$; ***$p < 0.001$; ****$p < 0.0001$; ns, not significant ($p > 0.05$).

absence of p97 inhibitors by confocal microscopy. We incubated HeLa cells with fluorescently labeled Tf for 5 min, washed away unbound Tf, and followed the time-dependent decay of fluorescence signals, which reflects Tf recycling and release to the medium (Figure 7A; Supplemental Figure S8). In control cells, most fluorescent Tf disappeared between 20 and 30 min after washout. By contrast, cells pretreated with CB-5083 and in particular NMS-873 showed residual Tf signals after 30 min, indicating delayed recycling. To obtain quantitative data, we determined the decay of Tf fluorescence over time by FACS analysis (Figure 7B). After

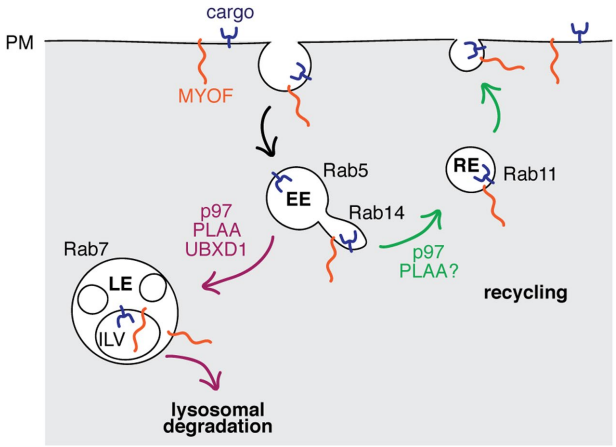

FIGURE 8: Schematic summarizing roles of p97 in endosomal trafficking. Cargo is endocytosed at the PM and delivered to an EEs. From the vacuolar domain of the EE, cargo is internalized into an ILV in a process dependent on p97 and its cofactors PLAA and UBXD1 (magenta pathway). The ILV-carrying endosome matures into a LE and subsequently fuses with lysosomes for cargo degradation. Alternatively, cargo is sorted from the tubular domain of the EE for recycling to the PM via a RE in a process involving p97 and presumably PLAA (green pathway). Key Rab protein characteristic for the distinct endosomal (sub)compartments are indicated. For the sake of clarity, (endo)lysosomes, intermediate compartments of the recycling pathway as well as the direct, rapid recycling from EEs to the PM have been omitted. MYOF is implicated in endocytosis, endolysosomal degradation, and endocytic recycling, but its precise function in these processes remain unknown.

normalization to the zero-minute timepoint, the inhibitor-treated cells showed a statistically significant delay in Tf recycling (Figure 7, C and D) with increased half-lives of ~ 33 (CB-5083) and 41 (NMS-873) min, compared with 29 min for control cells. Taken together, these results demonstrate that p97 is present at REs and that its activity is important for the efficient recycling of endocytic cargo.

DISCUSSION

In this study, we identified the membrane repair and trafficking factor MYOF as a novel, PLAA-dependent p97 interactor and showed that subpopulations of endogenous p97, PLAA, and MYOF associate with Rab11- and Rab14-positive, bona fide REs. Pharmacological inhibition stabilized the association of p97 with Tf-positive REs and delayed Tf recycling, demonstrating a role of p97 in the recycling of endocytic cargo.

p97 possesses multiple, mechanistically still poorly understood functions in endocytic trafficking (Figure 8). On the one hand, p97 was shown to restrict the size of EEs, presumably by controlling the oligomeric state of the Rab5 effector EEA1 (Ramanathan and Ye, 2012). On the other hand, expression of MSP1-causing mutant p97 as well as depletion of the p97 cofactor UBXD1 was shown to interfere with normal endolysosomal trafficking of caveolins, causing their accumulation at the limiting membrane of enlarged endosomal structures (Ritz *et al.*, 2011). Similarly, deletion of PLAA and expression of disease-linked mutant PLAA were shown to interfere with the recruitment of ESCRT-0 to EEs and with the formation of ILVs, resulting in the enrichment of EGF–EGFR cargo complexes at the endosomal membrane (Hall *et al.*, 2017). Taken together, the latter two studies establish that p97, UBXD1, and PLAA function in the sorting of endocytic cargo at/into the vacuolar domain of EEs and/or the formation of ILVs, thereby promoting lysosomal degradation. The present study adds another role for p97 in endocytic trafficking, as p97 also associates with REs (Figures 4 and 6) and p97 activity is needed for the efficient recycling of endocytic cargo (Figure 7). While an involvement of p97 in Tf recycling has been proposed before (Ramanathan and Ye, 2012), it should be noted that this claim was solely based on an experiment employing the small-molecule inhibitor eeyarestatin I (EerI), which in addition to p97 potently inhibits Sec61-dependent protein translocation, thereby inducing rapid Ca^{2+} leakage from the endoplasmic reticulum (Gamayun *et al.*, 2019). Thus, it cannot be ruled out that the effects of EerI on Tf recycling observed by Ramanathan and Ye were actually caused by elevated cytosolic Ca^{2+} concentrations or a perturbed secretory pathway. By contrast, our qualitative and quantitative assays demonstrate that the two state-of-the-art p97 inhibitors, NMS-873 and CB-5083, induce a delayed recycling of Tf, thus reliably establishing a function of p97 in endocytic recycling. Together with the recently identified roles of p97 in the removal of damaged lysosomes by selective autophagy (Papadopoulos *et al.*, 2017) and in the dynamics of tubular lysosomal structures in fly muscle (Johnson *et al.*, 2015), p97 has thus emerged as a key factor in endosomal trafficking and lysosomal homeostasis.

The precise function of p97 in endocytic recycling remains unclear. The association of the ubiquitin-binding cofactor PLAA with REs (Figure 5, C–F) and the PLAA-dependent interaction between p97 and MYOF (Figure 5, A and B) suggest an involvement of the ubiquitin system. However, while the posttranslational modification with ubiquitin is a well-established sorting signal for the ESCRT-mediated internalization of endocytic cargo into ILVs (Raiborg and Stenmark, 2009), no unifying model for the role(s) of the ubiquitin system in endocytic recycling has emerged yet (Berlin *et al.*, 2023). Of note, it has been shown that HACE1-mediated ubiquitylation activates Rab11 to promote the normal endocytic recycling of CD71 and the β2-adrenergic receptor (Lachance *et al.*, 2014). Moreover, the RE-associated Rab11 effectors Rab11-FIP1/2, EHD1, and MICALL1 have been reported to be ubiquitylated by RFFL and other E3 ligases (Sakai *et al.*, 2019), and the modification of the Wiskott-Aldrich syndrome protein and SCAR homolog (WASH) complex subunit WASH1 with K63-linked ubiquitin chains by the E3 ligase MAGE-L2-TRIM27 activates WASH to nucleate actin polymerization at REs (Hao *et al.*, 2013). Interestingly, the WASH subunit WASHC5/Strumpellin was previously identified as a p97 interactor (Clemen *et al.*, 2010), raising the interesting possibility that p97 could be involved in WASH complex activation. For the novel p97 interactor MYOF, 77 ubiquitylation sites identified in various global proteomics projects are annotated in the BioGRID database (Oughtred *et al.*, 2021). However, we failed to obtain direct evidence for a substantial ubiquitylation of endogenous MYOF, and treatment with pharmacological inhibitors of the 26S proteasome, p97, the ubiquitin E1 enzyme or deubiquitylating enzymes did not result in significant changes of total MYOF levels (unpublished data). While these findings make a role of p97 and the ubiquitin system in the degradation of bulk MYOF unlikely, they do not exclude the possibility that a subpopulation of MYOF is degraded in a ubiquitin- and/or p97-dependent manner, or that MYOF is (multiply?) monoubiquitylated in a nonproteolytic context. Alternatively, p97 and MYOF may be part of a protein complex at early or recycling endosomal compartments that is involved in cargo sorting/recycling. In support of this possibility, MYOF was shown to prevent the ubiquitylation and degradation of the constitutively recycled vascular endothelial growth factor receptor VEGFR2 (Bernatchez *et al.*, 2007) and to promote Tf recycling together with EHD2 (Doherty *et al.*, 2008). In either case, the

identities of (ubiquitylated) p97 targets critical for endocytic recycling remain to be determined.

Interestingly, a truncating *MYOF* mutation was recently identified in a patient presenting with a combination of cardiomyopathy and limb-girdle type muscular dystrophy (Kiselev *et al.*, 2019). This adds *MYOF* to the growing list of genes linked to endosomal processes that are mutated in neuromuscular disorders, including *VCP* (Pfeffer *et al.*, 2022), *PLAA* (Hall *et al.*, 2017), *CHMP2B* encoding an ESCRT-III subunit (Skibinski *et al.*, 2005), *WASHC4* encoding Swip (Gangfuss *et al.*, 2022), *WASHC5* encoding Strumpellin (Valdmanis *et al.*, 2007), and many others (Toupenet Marchesi *et al.*, 2021; Garcia-Cazorla *et al.*, 2022), which emphasize the high medical relevance of endosomal pathways and may suggest overlapping functions for some of the affected gene products. Our study linking p97, PLAA, and MYOF is in line with this suggestion and provides a starting point for future mechanistic analyses.

MATERIALS AND METHODS

All materials used, including antibodies, cell lines, and reagents, are listed in Supplemental Table S1.

Mammalian cell culture

HeLa cells (ATCC; CCL-2) and their derivatives, A549 (ATCC; CCL-185), and HEK293T (ATCC; CRL-3216) cells were cultured in Dulbecco's modified Eagle's medium (DMEM) supplemented with 10% fetal bovine serum and 1% penicillin/ streptomycin in a humidified atmosphere with 5% CO_2 at 37°C. Additional antibiotics were added to the culture media for HeLa pINDUCER20 cell pools (400 µg/ml G418) and HeLa KO cell pools (2 µg/ml puromycin). Cell lines were tested for mycoplasma contamination every 4–6 mo.

To generate HeLa cell pools ectopically expressing p97, coding sequences for wild-type and ATPase-deficient p97 including an N-terminal FLAG epitope tag were cloned into the lentiviral vector pINDUCER20 (Addgene plasmid #44012; gift from Stephen Elledge; Meerbrey *et al.*, 2011). After production of recombinant lentiviruses in HEK293T cells by cotransfection of the pINDUCER20 constructs with pMD2.G and psPAX2 (Addgene plasmids #12259 and #12260; gifts from Didier Trono), HeLa cells at 40–60% confluence were transduced with lentivirus-containing supernatant mixed with polybrene to a final concentration of 8 µg/ml. Twenty hours after transduction, fresh culture medium containing 1 mg/ml G418 was added and selection was performed for 12 d. Expression of FLAG-tagged p97 variants was induced by addition of 500 ng/ml doxycycline for 22 h.

To generate HeLa KO cell pools, recombinant lentiviruses were produced as described above using pools of 3–4 pLentiCRISPRv2-derived plasmids encoding gRNAs targeting the human *PLAA* and *VCP* genes, respectively (Wegner *et al.*, 2019; gift from Manuel Kaulich). The following gRNA sequences were used: PLAA-KO-1-R_21, CCGGTGGCAATTAGGCCATG; PLAA-KO-2-R_132, CTGATAGGCTTCGACTTTCT; PLAA-KO-3-R_35, GAGTTGATCCATTTACAGGT; PLAA-KO-4-R_2, TGGTTAACTGCATACAACTT; VCP-KO-2-R_86, CCGATGTCTTCCCAGGTTAC; VCP-KO-3-R_143, CTTCGCAGTGGATCACTGTG; VCP-KO-4-R_171,ACATGCC CGTGAGTCTCATT; Non-Human-Target-309-KO-1-R_156, AACATGACGTTCAAGATTGG; Non-Human-Target-365-KO-5-R_5, ACCACTGTTCTACGCGCAGG; Non-Human-Target-415-KO-2-R_24, TTGAACGGGCCGCGGAAGCG; Non-Human-Target-42-KO-15-R_115, CCCGCATGACACCGTCACTT. Recombinant lentiviruses were used to transduce HeLa cells as described above. Forty-eight hours after transduction, fresh culture medium containing 2 µg/ml puromycin was added, and the cell pools were kept under constant selection.

For the ectopic expression of MYOF-HA (pCDNA3.1-MYOF-HA; Addgene plasmid #22443; gift from William Sessa; Bernatchez *et al.*, 2007), GFP-Rab5WT (pEGFP-Rab5; Addgene plasmid #49888; gift from Marci Scidmore), GFP-Rab5QL (pEGFP-Rab5CA(QL); Addgene plasmid #35140; gift from Sergio Grinstein; Bohdanowicz *et al.*, 2012), GFP-Rab7 (pEGFP-Rab7; gift from Reinhard Jahn; Pavlos *et al.*, 2010), GFP-Rab11 (pEGFP-Rab11; Addgene plasmid #12674; gift from Richard Pagano; Choudhury *et al.*, 2002), and GFP-Rab14 (pEGFP-Rab14; gift from Reinhard Jahn; Pavlos *et al.*, 2010), cells were transfected at 50% confluence using polyethylenimine and analyzed 24 h (immunofluorescence) or 48 h (IP) after transfection. For siRNA-mediated depletions, cells were seeded in 12-well plates and transfected with 50 nM siRNA using 1.5 µl Oligofectamine (Thermo Fisher) diluted in 125 µl Opti-MEM per well in a final volume of 1 ml. After 20 h, the medium was changed and the knockdown was continued for a total of 72 h.

In-cell crosslinking

Cells were grown to 80–90% confluence on 15-cm dishes, washed two times with phosphate-buffered saline (PBS), and incubated with DSP (0.8 mM final conc. in PBS) for 30 min at room temperature. Then, the crosslinker was quenched with 25 mM Tris/HCl pH 7.6 for 10 min at room temperature and the supernatant was removed. The cells were collected in PBS, harvested by centrifugation, and the cell pellet was flash frozen in liquid nitrogen and stored at -80°C.

IP experiments

For IP of p97 or MYOF, the frozen pellets of crosslinked cells were resuspended in lysis buffer (50 mM Tris pH 7.6, 150 mM NaCl, 2 mM $MgCl_2$, 1% Nonidet P40, 10% glycerol) containing protease inhibitors (1 mM PMSF, 1× Roche complete protease inhibitor mix) and incubated for 10 min on ice. Cell debris was removed by centrifugation, and the protein concentration of the supernatants was determined with the 660 nm Protein Assay Kit (Pierce) and adjusted to same input levels as appropriate. Supernatants were precleared by incubation with 20 µl of protein G sepharose beads (1 h, 4°C) on a rotating wheel. The precleared supernatants were incubated with specific antibodies as indicated (p97, HA: 6 µg; MYOF: 10 µg) or with the appropriate unspecific control IgGs (IgG, rabbit; IgG2a, mouse) for 1 h at 4°C on a rotating wheel, before 25 µl of protein G sepharose beads were added for 2 h at 4°C. The beads were washed twice with lysis buffer containing protease inhibitors, once with lysis buffer without inhibitors, and once with Tris-buffered saline (TBS). The immunoprecipitates were heat-denatured on the beads in sample buffer, separated by SDS–PAGE and further analyzed by mass spectrometry or immunoblotting. For immunoblot analysis, 1–2% of the total soluble lysate were loaded as inputs, and 20–25% of the total immunoprecipitates were loaded as IP samples.

Mass spectrometry

Proteins in NuPAGE LDS sample buffer (Life Technologies) were reduced with 50 mM DTT at 70°C for 10 min, alkylated with 120 mM iodoacetamide at room temperature for 20 min, and separated on NuPAGE Novex 4–12% Bis-Tris gels (Life Technologies) in MOPS buffer according to manufacturer's instructions. Gels were washed three times for 5 min with water and stained for 45 min with Simply Blue Safe Stain (Life Technologies). After washing with water for 2 h, each gel lane was cut into 15 slices. For in-gel digestion, the excised gel slices were destained with 30% acetonitrile, shrunk with 100% acetonitrile, and dried in a vacuum concentrator. Trypsin digest was performed overnight at 37°C in 0.05 M NH_4HCO_3 (pH 8), using

0.1 µg of protease per slice. Peptides were extracted from the gel slices with 5% formic acid.

NanoLC-MS/MS analyses were performed on an Orbitrap Fusion (Thermo Fisher Scientific) equipped with a PicoView Ion Source (New Objective) and coupled to an EASY-nLC 1000 (Thermo Fisher Scientific). Peptides were loaded on capillary columns (PicoFrit, 30 cm × 150 µm ID, New Objective) packed with ReproSil-Pur 120 C18-AQ 1.9 µm (Dr. Maisch), and separated with a 30 min linear gradient from 3 to 30% acetonitrile and 0.1% formic acid at a flow rate of 500 nl/min. Both MS and MS/MS scans were acquired in the Orbitrap analyzer with a resolution of 60,000 for MS scans and 15,000 for MS/MS scans. HCD fragmentation with 35% normalized collision energy was applied. A Top Speed data-dependent MS/MS method with a fixed cycle time of 3 s was used. Dynamic exclusion was applied with a repeat count of 1 and an exclusion duration of 120 s; singly charged precursors were excluded from selection. Minimum signal threshold for precursor selection was set to 50,000. Predictive AGC was used with a target value of 5e5 for MS scans and 5e4 for MS/MS scans. EASY-IC was used for internal calibration.

For raw data file processing, database searches and quantification, MaxQuant version 1.5.7.4 was used (Cox and Mann, 2008). The search was performed against the *Homo sapiens* reference proteome database (Uniprot, UP000005640, 78,120 entries, download date 2021-09-09) and, additionally, a database containing common cell culture contaminants. The search was performed with tryptic cleavage specificity with three allowed miscleavages. Protein identification was under control of the false-discovery rate (FDR) (<1% false-discovery rate on protein and peptide level). In addition to MaxQuant default settings, the search was performed allowing the following variable modifications: Protein N-terminal acetylation, Gln to pyro-Glu formation (N-term; Gln), and oxidation (Met). For protein quantitation, the LFQ intensities were used (Cox *et al.*, 2014). Proteins with less than two identified razor/unique peptides were dismissed. The mass spectrometry proteomics data have been deposited to the ProteomeXchange Consortium via the PRIDE partner repository (Perez-Riverol *et al.*, 2022) with the dataset identifier PXD04116.

Further data analysis was performed using R scripts developed in-house. For discrimination of unspecifically immunoprecipitated proteins, LFQ intensities of IP control samples were quantile normalized, and median intensities were calculated. Missing LFQ intensities in the control samples were imputed with values close to the baseline. Data imputation was performed with values from a standard normal distribution with a mean of the 5% quantile of the combined log10-transformed LFQ intensities and a SD of 0.1. For the identification of significantly coimmunoprecipitated proteins, boxplot outliers were identified in intensity bins of at least 300 proteins. Log2 transformed protein ratios of IP versus control with values outside a 1.5× (potential) or 3× (extreme) interquartile range, respectively, were considered as coprecipitated with significance levels one and two, respectively.

Immunoblotting

For immunoblot analysis, cells were washed with PBS, resuspended in 1× Laemmli sample buffer (0.001% bromophenol blue, 10% glycerol, 2% SDS, 60 mM Tris-HCl, pH 6.8) supplemented with 100 mM DTT, and denatured at 95°C for 5 min. Proteins were resolved by SDS–PAGE and transferred onto PVDF membrane (Millipore) by semidry blotting using 1× Tris-glycine buffer (192 mM glycine, 25 mM Tris base, pH 8.3) supplemented with 20% methanol. The membrane was blocked with 5% milk in Tris-based saline with Tween (TBST) (50 mM Tris-HCl pH 7.5, 150 mM NaCl, 0.1% Tween 20) and incubated with the indicated primary antibody in blocking solution overnight at 4°C. The membrane was washed with TBST (3 × 5 min), incubated with HRP-conjugated secondary antibody (Dianova) diluted 1:10,000 in blocking solution for 1 h at room temperature (RT), washed again with TBST (3 × 10 min), and incubated with Clarity Western ECL Substrate (Bio-Rad). Chemiluminescence signals were detected using the Gel Doc XR+ system (Bio-Rad). Immunoblot images were processed by Image Lab software (Bio-Rad).

Immunofluorescence

Cells grown on coverslips to 60% confluence were washed twice with PBS, fixed using 3.7% formaldehyde in PBS for 12 min at RT, washed twice with cold PBS, permeabilized with 0.2% Triton X-100 and 1% bovine serum albumin (BSA) in PBS for 10 min at RT, washed with PBS, and blocked by incubation with 1% BSA in PBS for one hour at RT. Cells were incubated with the indicated primary antibodies (diluted in 1% BSA in PBS) overnight at 4°C, washed for 5 min with PBS, incubated with the appropriate fluorophore-coupled secondary antibodies for 2 h at RT, washed for 10 min with PBS, and rinsed with water. For coimmunostaining with the Alexa Fluor 647–p97 antibody conjugate, the conjugate was added together with the secondary antibodies. Coverslips were mounted for microscopy with mounting medium containing 4′,6-diamidino-2-phenylindole (DAPI; Vectashield) or with ProLong Glass Antifade Mountant and sealed with nail polish.

For Tf labeling, cells were washed twice with PBS and starved for 30 min in serum-free medium containing 25 mM HEPES pH 7.4 and 0.5% BSA. The cells were washed with cold PBS and labeled with 20 µg/ml Tf conjugated with Alexa Fluor 594 (Thermo Fisher; diluted in serum-free medium containing 25 mM HEPES pH 7.4 and 0.5% BSA) for 30 min at 37°C, washed twice with PBS and fixed. For Tf recycling experiments, cells were incubated with the Tf conjugate for 5 min at 37°C. The cells were washed with cold PBS and the coverslips were transferred to prewarmed growth medium and placed in the incubator. The cells were allowed to recycle Tf for the indicated times, washed twice with cold PBS and fixed for 15 min with 3.7% formaldehyde in PBS.

Microscopy and image processing

Confocal immunofluorescence microscopy was performed at the Imaging Core Facility (Biocenter, University of Würzburg) using a Leica TCS SP2 confocal microscope equipped with an acousto-optic beam splitter. Images were acquired using a 63×/1.4 oil immersion objective and Leica confocal software. Where higher resolution was required, 2× digital zooming was applied. Single planes or Z-stacks were acquired using diode UV (405 nm), Ar (488 nm), DPSS (561 nm) and HeNe (633 nm) lasers with PMTs set to 413–467 nm, 500–550 nm, 581–650 nm and 650–750 nm, respectively. Image processing was performed using Fiji (Schindelin *et al.*, 2012). Plot profiles along the arrows shown in the corresponding figures were generated using Fiji. For the object-based colocalization analysis of Figure 2, D–K, the images were autothresholded using the Renji-Entropy method after background substraction, and the Fiji plugin ComDet v.0.5.5 was applied to quantify structures in both channels as well as colocalizing puncta. In Figure 7A and Supplemental Figure S8, maximum intensity projections of five to six planes are shown.

FACS analysis of transferrin recycling

HeLa cells were grown on 15-cm dishes until 80–90% confluent. The medium was removed and fresh medium containing DSMO, NMS-873 (10 µM) or CB-5083 (10 µM) was added for 3.5 h. The cells were washed twice with PBS and starved for 30 min in serum-free medium containing 25 mM HEPES pH 7.4, 0.5% BSA and DSMO, NMS-873

or CB-5083 as appropriate. The cells were washed with PBS, incubated with 5 mM ethylenediaminetetraacetic acid in PBS for 5 min at 37°C, and the supernatant was removed. The cells were harvested, collected by centrifugation at 4°C and washed twice with cold PBS, before a control sample lacking transferrin was collected. Cell pellets were resuspended in 1 ml cold serum-free medium containing 25 mM HEPES pH 7.4, 0.5% BSA, 50 µg/ml transferrin conjugated with Alexa Fluor 594, and DSMO, NMS-873, or CB-5083 as appropriate. Cells were incubated at 37°C for 5 min and washed twice with cold PBS. Cell pellets were resuspended in prewarmed growth medium containing DSMO, NMS-873, or CB-5083 as appropriate. Cell samples were aliquoted and incubated for the indicated times at 37°C. Subsequently, the samples were washed twice with cold PBS, resuspended in 1 ml cold PBS and placed on ice. Transferrin fluorescence was measured on an AttuneTM NxT Acoustic Focusing Cytometer (laser: 561 nm, detector/channel: YL2; filter: 620/15 nm) using AttuneTM NxT Software. The mean signal (YL2-A) for 10,000 single cells was measured, background signal was subtracted and the data was normalized to the time point 0 min. Mean values and SDs were calculated from three independent biological replicates, and statistical significance was determined using a two-way ANOVA (Bonferroni's multiple comparison test). The data points were fitted to single exponential decay functions using GraphPad Prism 9.

ACKNOWLEDGMENTS

We thank Stephen Elledge, Sergio Grinstein, Reinhard Jahn, Manuel Kaulich, Richard Pagano, Marci Scidmore, William Sessa, and Didier Trono for providing plasmids; the Imaging Core Facility (Biocenter, University of Würzburg) for support with confocal and structured illumination microscopy; Thomas Rudel and Kathrin Stelzner (Chair of Microbiology, Biocenter, University of Würzburg) for access and introduction to the Attune FACS analyzer; Susanne Meyer for excellent technical assistance; and members of the Buchberger lab for critical reading of the manuscript. This work was supported by grants GRK2243/1+2 and BU951/5-1 of the Deutsche Forschungsgemeinschaft (to A.B.).

REFERENCES

Anderson DJ, Le Moigne R, Djakovic S, Kumar B, Rice J, Wong S, Wang J, Yao B, Valle E, Kiss von Soly S, *et al.* (2015). Targeting the AAA ATPase p97 as an approach to treat cancer through disruption of protein homeostasis. Cancer Cell 28, 653–665.

Balchin D, Hayer-Hartl M, Hartl FU (2016). In vivo aspects of protein folding and quality control. Science 353, aac4354.

Berlin I, Sapmaz A, Stevenin V, Neefjes J (2023). Ubiquitin and its relatives as wizards of the endolysosomal system. J Cell Sci 136.

Bernatchez PN, Acevedo L, Fernandez-Hernando C, Murata T, Chalouni C, Kim J, Erdjument-Bromage H, Shah V, Gratton JP, McNally EM, *et al.* (2007). Myoferlin regulates vascular endothelial growth factor receptor-2 stability and function. J Biol Chem 282, 30745–30753.

Bernatchez PN, Sharma A, Kodaman P, Sessa WC (2009). Myoferlin is critical for endocytosis in endothelial cells. Am J Physiol Cell Physiol 297, C484–492.

Bodnar N, Rapoport T (2017). Toward an understanding of the Cdc48/p97 ATPase. F1000Res 6, 1318.

Bohdanowicz M, Balkin DM, De Camilli P, Grinstein S (2012). Recruitment of OCRL and Inpp5B to phagosomes by Rab5 and APPL1 depletes phosphoinositides and attenuates Akt signaling. Mol Biol Cell 23, 176–187.

Brandman O, Stewart-Ornstein J, Wong D, Larson A, Williams CC, Li GW, Zhou S, King D, Shen PS, Weibezahn J, *et al.* (2012). A ribosome-bound quality control complex triggers degradation of nascent peptides and signals translation stress. Cell 151, 1042–1054.

Buchan JR, Kolaitis RM, Taylor JP, Parker R (2013). Eukaryotic stress granules are cleared by autophagy and Cdc48/VCP function. Cell 153, 1461–1474.

Buchberger A (2022). Unfolding by Cdc48/p97: different strokes for different folks. Trends Cell Biol 32, 278–280.

Buchberger A, Bukau B, Sommer T (2010). Protein quality control in the cytosol and the endoplasmic reticulum: brothers in arms. Mol Cell 40, 238–252.

Buchberger A, Schindelin H, Hanzelmann P (2015). Control of p97 function by cofactor binding. FEBS Lett 589, 2578–2589.

Bulankina AV, Thoms S (2020). Functions of vertebrate ferlins. Cells 9, 534.

Choudhury A, Dominguez M, Puri V, Sharma DK, Narita K, Wheatley CL, Marks DL, Pagano RE (2002). Rab proteins mediate Golgi transport of caveola-internalized glycosphingolipids and correct lipid trafficking in Niemann-Pick C cells. J Clin Invest 109, 1541–1550.

Clague MJ, Urbe S (2010). Ubiquitin: same molecule, different degradation pathways. Cell 143, 682–685.

Clemen CS, Tangavelou K, Strucksberg KH, Just S, Gaertner L, Regus-Leidig H, Stumpf M, Reimann J, Coras R, Morgan RO, *et al.* (2010). Strumpellin is a novel valosin-containing protein binding partner linking hereditary spastic paraplegia to protein aggregation diseases. Brain 133, 2920–2941.

Cox J, Hein MY, Luber CA, Paron I, Nagaraj N, Mann M (2014). Accurate proteome-wide label-free quantification by delayed normalization and maximal peptide ratio extraction, termed MaxLFQ. Molecular Cellular Proteomics: MCP 13, 2513–2526.

Cox J, Mann M (2008). MaxQuant enables high peptide identification rates, individualized p.p.b.-range mass accuracies and proteome-wide protein quantification. Nat Biotechnol 26, 1367–1372.

Cullen PJ, Steinberg F (2018). To degrade or not to degrade: mechanisms and significance of endocytic recycling. Nat Rev Mol Cell Biol 19, 679–696.

Dantuma NP, Hoppe T (2012). Growing sphere of influence: Cdc48/p97 orchestrates ubiquitin-dependent extraction from chromatin. Trends Cell Biol 22, 483–491.

Demonbreun AR, Lapidos KA, Heretis K, Levin S, Dale R, Pytel P, Svensson EC, McNally EM (2010a). Myoferlin regulation by NFAT in muscle injury, regeneration and repair. J Cell Sci 123, 2413–2422.

Demonbreun AR, Posey AD, Heretis K, Swaggart KA, Earley JU, Pytel P, McNally EM (2010b). Myoferlin is required for insulin-like growth factor response and muscle growth. FASEB J 24, 1284–1295.

Dikic I (2017). Proteasomal and autophagic degradation systems. Annu Rev Biochem 86, 193–224.

Doherty KR, Cave A, Davis DB, Delmonte AJ, Posey A, Earley JU, Hadhazy M, McNally EM (2005). Normal myoblast fusion requires myoferlin. Development 132, 5565–5575.

Doherty KR, Demonbreun AR, Wallace GQ, Cave A, Posey AD, Heretis K, Pytel P, McNally EM (2008). The endocytic recycling protein EHD2 interacts with myoferlin to regulate myoblast fusion. J Biol Chem 283, 20252–20260.

Gamayun I, O'Keefe S, Pick T, Klein MC, Nguyen D, McKibbin C, Piacenti M, Williams HM, Flitsch SL, Whitehead RC, *et al.* (2019). Eeyarestatin compounds selectively enhance Sec61-mediated Ca(2+) leakage from the endoplasmic reticulum. Cell Chem Biol 26, 571–583 e576.

Gangfuss A, Czech A, Hentschel A, Munchberg U, Horvath R, Topf A, O'Heir E, Lochmuller H, Stehling F, Kiewert C, *et al.* (2022). Homozygous WASHC4 variant in two sisters causes a syndromic phenotype defined by dysmorphisms, intellectual disability, profound developmental disorder, and skeletal muscle involvement. J Pathol 256, 93–107.

Garcia-Cazorla A, Oyarzabal A, Saudubray JM, Martinelli D, Dionisi-Vici C (2022). Genetic disorders of cellular trafficking. Trends Genet 38, 724–751.

Grant BD, Donaldson JG (2009). Pathways and mechanisms of endocytic recycling. Nat Rev Mol Cell Biol 10, 597–608.

Hall EA, Nahorski MS, Murray LM, Shaheen R, Perkins E, Dissanayake KN, Kristaryanto Y, Jones RA, Vogt J, Rivagorda M, *et al.* (2017). PLAA mutations cause a lethal infantile epileptic encephalopathy by disrupting ubiquitin-mediated endolysosomal degradation of synaptic proteins. Am J Hum Genet 100, 706–724.

Hao YH, Doyle JM, Ramanathan S, Gomez TS, Jia D, Xu M, Chen ZJ, Billadeau DD, Rosen MK, Potts PR (2013). Regulation of WASH-dependent actin polymerization and protein trafficking by ubiquitination. Cell 152, 1051–1064.

Her NG, Toth JI, Ma CT, Wei Y, Motamedchaboki K, Sergienko E, Petroski MD (2016). p97 composition changes caused by allosteric inhibition are suppressed by an on-target mechanism that increases the enzyme's ATPase activity. Cell Chem Biol 23, 517–528.

Hershko A, Ciechanover A (1992). The ubiquitin system for protein degradation. Annu Rev Biochem 61, 761–807.

Huang EY, To M, Tran E, Dionisio LTA, Cho HJ, Baney KLM, Pataki CI, Olzmann JA (2018). A VCP inhibitor substrate trapping approach (VISTA)

enables proteomic profiling of endogenous ERAD substrates. Mol Biol Cell 29, 1021–1030.
Huotari J, Helenius A (2011). Endosome maturation. EMBO J 30, 3481–3500.
Johnson AE, Shu H, Hauswirth AG, Tong A, Davis GW (2015). VCP-dependent muscle degeneration is linked to defects in a dynamic tubular lysosomal network in vivo. eLife 4, e07366.
Johnson JO, Mandrioli J, Benatar M, Abramzon Y, Van Deerlin VM, Trojanowski JQ, Gibbs JR, Brunetti M, Gronka S, Wuu J, *et al.* (2010). Exome sequencing reveals VCP mutations as a cause of familial ALS. Neuron 68, 857–864.
Ju JS, Miller SE, Hanson PI, Weihl CC (2008). Impaired protein aggregate handling and clearance underlie the pathogenesis of p97/VCP-associated disease. J Biol Chem 283, 30289–30299.
Kim NC, Tresse E, Kolaitis RM, Molliex A, Thomas RE, Alami NH, Wang B, Joshi A, Smith RB, Ritson GP, *et al.* (2013). VCP is essential for mitochondrial quality control by PINK1/Parkin and this function is impaired by VCP mutations. Neuron 78, 65–80.
Kiselev A, Vaz R, Knyazeva A, Sergushichev A, Dmitrieva R, Khudiakov A, Jorholt J, Smolina N, Sukhareva K, Fomicheva Y, *et al.* (2019). Truncating variant in Myof gene is associated with limb-girdle type muscular dystrophy and cardiomyopathy. Front Genet 10, 608.
Labbadia J, Morimoto RI (2015). The biology of proteostasis in aging and disease. Annu Rev Biochem 84, 435–464.
Lachance V, Degrandmaison J, Marois S, Robitaille M, Genier S, Nadeau S, Angers S, Parent JL (2014). Ubiquitylation and activation of a Rab GTPase is promoted by a beta(2)AR-HACE1 complex. J Cell Sci 127, 111–123.
Lamark T, Johansen T (2021). Mechanisms of selective autophagy. Annu Rev Cell Dev Biol 37, 143–169.
Lamber EP, Siedenburg AC, Barr FA (2019). Rab regulation by GEFs and GAPs during membrane traffic. Curr Opin Cell Biol 59, 34–39.
Langemeyer L, Frohlich F, Ungermann C (2018). Rab GTPase function in endosome and lysosome biogenesis. Trends Cell Biol 28, 957–970.
Linford A, Yoshimura S, Nunes Bastos R, Langemeyer L, Gerondopoulos A, Rigden DJ, Barr FA (2012). Rab14 and its exchange factor FAM116 link endocytic recycling and adherens junction stability in migrating cells. Dev Cell 22, 952–966.
Magnaghi P, D'Alessio R, Valsasina B, Avanzi N, Rizzi S, Asa D, Gasparri F, Cozzi L, Cucchi U, Orrenius C, *et al.* (2013). Covalent and allosteric inhibitors of the ATPase VCP/p97 induce cancer cell death. Nature chemical biology 9, 548–556.
Mayle KM, Le AM, Kamei DT (2012). The intracellular trafficking pathway of transferrin. Biochim Biophys Acta 1820, 264–281.
Meerbrey KL, Hu G, Kessler JD, Roarty K, Li MZ, Fang JE, Herschkowitz JI, Burrows AE, Ciccia A, Sun T, *et al.* (2011). The pINDUCER lentiviral toolkit for inducible RNA interference in vitro and in vivo. Proc Natl Acad Sci USA 108, 3665–3670.
Oughtred R, Rust J, Chang C, Breitkreutz BJ, Stark C, Willems A, Boucher L, Leung G, Kolas N, Zhang F, *et al.* (2021). The BioGRID database: A comprehensive biomedical resource of curated protein, genetic, and chemical interactions. Protein Sci 30, 187–200.
Papadopoulos C, Kirchner P, Bug M, Grum D, Koerver L, Schulze N, Poehler R, Dressler A, Fengler S, Arhzaouy K, *et al.* (2017). VCP/p97 cooperates with YOD1, UBXD1 and PLAA to drive clearance of ruptured lysosomes by autophagy. EMBO J 36, 135–150.
Papadopoulos C, Meyer H (2017). Detection and clearance of damaged lysosomes by the endo-lysosomal damage response and lysophagy. Curr Biol 27, R1330–R1341.
Pavlos NJ, Grønborg M, Riedel D, Chua JJ, Boyken J, Kloepper TH, Urlaub H, Rizzoli SO, Jahn R. (2010). Quantitative analysis of synaptic vesicle Rabs uncovers distinct yet overlapping roles for Rab3a and Rab27b in Ca2+-triggered exocytosis. J Neurosci 30, 13441–13453.
Perez-Riverol Y, Bai J, Bandla C, Garcia-Seisdedos D, Hewapathirana S, Kamatchinathan S, Kundu DJ, Prakash A, Frericks-Zipper A, Eisenacher M, *et al.* (2022). The PRIDE database resources in 2022: a hub for mass spectrometry-based proteomics evidences. Nucleic Acids Res 50, D543–D552.
Pfeffer G, Lee G, Pontifex CS, Fanganiello RD, Peck A, Weihl CC, Kimonis V (2022). Multisystem proteinopathy due to VCP mutations: a review of clinical heterogeneity and genetic diagnosis. Genes (Basel) 13, 963.
Raiborg C, Stenmark H (2009). The ESCRT machinery in endosomal sorting of ubiquitylated membrane proteins. Nature 458, 445–452.
Ramanathan HN, Ye Y. (2012). The p97 ATPase associates with EEA1 to regulate the size of early endosomes. Cell Res 22, 346–359.
Redpath GM, Sophocleous RA, Turnbull L, Whitchurch CB, Cooper ST (2016). Ferlins show tissue-specific expression and segregate as plasma membrane/late endosomal or trans-Golgi/recycling ferlins. Traffic 17, 245–266.
Ritz D, Vuk M, Kirchner P, Bug M, Schutz S, Hayer A, Bremer S, Lusk C, Baloh RH, Lee H, *et al.* (2011). Endolysosomal sorting of ubiquitylated caveolin-1 is regulated by VCP and UBXD1 and impaired by VCP disease mutations. Nat Cell Biol 13, 1116–1123.
Rodriguez-Ortiz CJ, Flores JC, Valenzuela JA, Rodriguez GJ, Zumkehr J, Tran DN, Kimonis VE, Kitazawa M (2016). The myoblast C2C12 transfected with mutant valosin-containing protein exhibits delayed stress granule resolution on oxidative stress. Am J Pathol 186, 1623–1634.
Sakai R, Fukuda R, Unida S, Aki M, Ono Y, Endo A, Kusumi S, Koga D, Fukushima T, Komada M, *et al.* (2019). The integral function of the endocytic recycling compartment is regulated by RFFL-mediated ubiquitylation of Rab11 effectors. J Cell Sci 132, jcs228007.
Schindelin J, Arganda-Carreras I, Frise E, Kaynig V, Longair M, Pietzsch T, Preibisch S, Rueden C, Saalfeld S, Schmid B, *et al.* (2012). Fiji: an open-source platform for biological-image analysis. Nat Methods 9, 676–682.
Skibinski G, Parkinson NJ, Brown JM, Chakrabarti L, Lloyd SL, Hummerich H, Nielsen JE, Hodges JR, Spillantini MG, Thusgaard T, *et al.* (2005). Mutations in the endosomal ESCRTIII-complex subunit CHMP2B in frontotemporal dementia. Nat Genet 37, 806–808.
Tanaka A, Cleland MM, Xu S, Narendra DP, Suen DF, Karbowski M, Youle RJ. (2010). Proteasome and p97 mediate mitophagy and degradation of mitofusins induced by Parkin. J Cell Biol 191, 1367–1380.
Toupenet Marchesi L, Leblanc M, Stevanin G (2021). Current knowledge of endolysosomal and autophagy defects in hereditary spastic paraplegia. Cells 10, 1678.
Turakhiya A, Meyer SR, Marincola G, Bohm S, Vanselow JT, Schlosser A, Hofmann K, Buchberger A (2018). ZFAND1 recruits p97 and the 26S proteasome to promote the clearance of arsenite-induced stress granules. Mol Cell 70, 906–919.
Turtoi A, Blomme A, Bellahcene A, Gilles C, Hennequiere V, Peixoto P, Bianchi E, Noel A, De Pauw E, Lifrange E, *et al.* (2013). Myoferlin is a key regulator of EGFR activity in breast cancer. Cancer Res 73, 5438–5448.
Ullrich O, Reinsch S, Urbe S, Zerial M, Parton RG (1996). Rab11 regulates recycling through the pericentriolar recycling endosome. J Cell Biol 135, 913–924.
Valdmanis PN, Meijer IA, Reynolds A, Lei A, MacLeod P, Schlesinger D, Zatz M, Reid E, Dion PA, Drapeau P, *et al.* (2007). Mutations in the KIAA0196 gene at the SPG8 locus cause hereditary spastic paraplegia. Am J Hum Genet 80, 152–161.
van den Boom J, Meyer H (2018). VCP/p97-mediated unfolding as a principle in protein homeostasis and signaling. Mol Cell 69, 182–194.
van der Sluijs P, Hull M, Webster P, Male P, Goud B, Mellman I (1992). The small GTP-binding protein rab4 controls an early sorting event on the endocytic pathway. Cell 70, 729–740.
Wandinger-Ness A, Zerial M (2014). Rab proteins and the compartmentalization of the endosomal system. Cold Spring Harbor perspectives in biology 6, a022616.
Wang B, Maxwell BA, Joo JH, Gwon Y, Messing J, Mishra A, Shaw TI, Ward AL, Quan H, Sakurada SM, *et al.* (2019). ULK1 and ULK2 regulate stress granule disassembly through phosphorylation and activation of VCP/p97. Mol Cell 74, 742–757.
Watts GD, Wymer J, Kovach MJ, Mehta SG, Mumm S, Darvish D, Pestronk A, Whyte MP, Kimonis VE (2004). Inclusion body myopathy associated with Paget disease of bone and frontotemporal dementia is caused by mutant valosin-containing protein. Nat Genet 36, 377–381.
Wegner M, Diehl V, Bittl V, de Bruyn R, Wiechmann S, Matthess Y, Hebel M, Hayes MG, Schaubeck S, Benner C, *et al.* (2019). Circular synthesized CRISPR/Cas gRNAs for functional interrogations in the coding and noncoding genome. eLife 8, e42549.
Xue L, Blythe EE, Freiberger EC, Mamrosh JL, Hebert AS, Reitsma JM, Hess S, Coon JJ, Deshaies RJ (2016). Valosin-containing protein (VCP)-adaptor interactions are exceptionally dynamic and subject to differential modulation by a VCP inhibitor. Molecular & Cellular Proteomics: MCP 15, 2970–2986.
Ye Y, Meyer HH, Rapoport TA (2001). The AAA ATPase Cdc48/p97 and its partners transport proteins from the ER into the cytosol. Nature 414, 652–656.
Ye Y, Meyer HH, Rapoport TA (2003). Function of the p97-Ufd1-Npl4 complex in retrotranslocation from the ER to the cytosol: dual recognition of nonubiquitinated polypeptide segments and polyubiquitin chains. J Cell Biol 162, 71–84.
Zhang T, Mishra P, Hay BA, Chan D, Guo M (2017). Valosin-containing protein (VCP/p97) inhibitors relieve Mitofusin-dependent mitochondrial defects due to VCP disease mutants. eLife 6, e17834.